eJSSNT Technical Note

e-Journal of Surface Science and Nanotechnology **21**, XX−XX (2023)

Developing a Simple Scanning Probe System for Soft X-ray Spectroscopy with a Nano-focusing Mirror

Hiroshi Ando,[a] Masafumi Horio,[a, †] Yoko Takeo,[a] Masahito Niibe,[a] Tetsuya Wada,[a] Yasunobu Ando,[b] Takahiro Kondo,[c, d] Takashi Kimura,[a] Iwao Matsuda [a]

[a] *Institute for Solid State Physics (ISSP), The University of Tokyo, Kashiwa, Chiba 277-8581, Japan*
[b] *Research Center for Computational Design of Advanced Functional Materials (CD-FMat), National Institute of Advanced Industrial Science and Technology (AIST), Tsukuba, Ibaraki 305-8568, Japan*
[c] *Faculty of Pure and Applied Sciences and R&D Center for Zero CO_2 Emission with Functional Materials, University of Tsukuba, Tsukuba 305-8573, Japan*
[d] *The Advanced Institute for Materials Research, Tohoku University, Sendai 980-8577, Japan*
[†] *Corresponding author: mhorio@issp.u-tokyo.ac.jp*

Received: 5 October, 2022; Accepted: 10 January, 2023; Advance Publication: 18 February, 2023; Published: 18 February, 2023

We developed a compact system for the spectroscopic mapping of a microstructure with a nano-focused beam at a soft X-ray beamline of synchrotron radiation. The experimental setup comprises a Wolter mirror and sample that are arranged with two mounting stages. The Wolter mirror is aligned with three degrees of freedom, and the sample with two degrees. The system generates a beam with an 800-nm spot and maps out a chemical distribution of non-uniform material through near-edge X-ray fine structure spectroscopy. The design and actual system are suited to experiments conducted with a nano-focused X-ray beam at beamlines of synchrotron radiation or an X-ray free-electron laser. Additionally, this technical note presents guidelines for actual experiments.

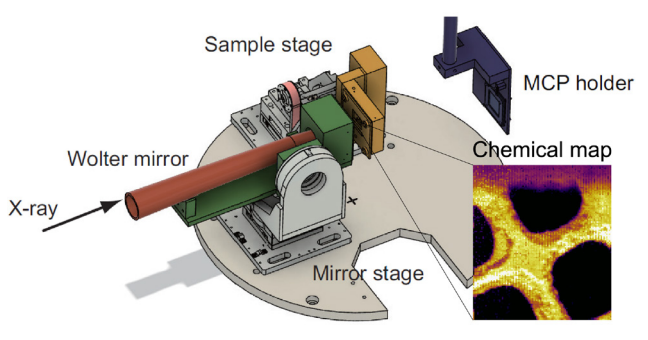

Keywords *X-ray spectroscopy; Nano-focusing mirror; Chemical map; Synchrotron radiation*

I. INTRODUCTION

Nanotechnology has advanced rapidly through the fabrication and assembly of functional materials in spaces of micrometer to nanometer scale. Developing such tiny materials requires accurate and quantitative characterizations of the composing elements and the individual chemical states. X-ray spectroscopic methods, such as X-ray absorption spectroscopy and photoelectron spectroscopy, have been effective in conducting these characterizations [1−3]. However, a conventional X-ray tube in a laboratory has a spot size on the order of a millimeter, and the obtained information is thus averaged over the microscopic sample.

Synchrotron radiation, as a highly brilliant and *hv*-tunable X-ray source, has been used for material characterizations with a spot size of below 100 μm at a beamline experimental station at SPring-8 BL07LSU [4−6]. The beam has been small enough to investigate varieties of micrometer-scale samples, but a further reduction of beam size is needed to examine a wider range of materials with finer structures or smaller size.

Recently, sub-micron and nanometer-scale X-ray beams have been generated at synchrotron radiation or X-ray free-electron laser beamlines using a Fresnel zone plate (FZP) [7−10], Kirkpatrick-Baez (KB) mirrors [11], Schwarzschild optics (SOs) [12, 13], capillary optics [14, 15], ellipsoidal mirror [16−19], and Wolter mirror [20−24]. Each optic has its advantages and disadvantages, and their characteristics should be taken into account when employing them in experimental systems. The FZP is now generally used for nano-focusing and can provide the focus spot sizes down to < 100 nm, but the FZP has chromatic aberration, a low focusing efficiency, and a short work distance. The KB mirrors have a high focusing efficiency and long work distance, do

not exhibit chromatic aberration, and the processing technology has been well-established, but the KB mirrors are usually composed of horizontal and vertical mirrors, so two mirror stages are needed for alignment. The SOs have a good aberration because of the normal incidence optic, but their usage is limited depending on the availability of high-reflective multilayers in the target energy range. Also, the narrow reflective band makes it unsuitable for wide-range measurements like the near-edge X-ray absorption fine structure (NEXAFS). The capillary has a compact form, which allows for flexibility in the system design, but the work distance is shorter than the other cylindrical rotationally symmetric mirrors and needs a central stop that decrees efficiency. The ellipsoidal mirror and the Wolter mirror are challenging to fabricate, but recent technological development has greatly advanced the quality of the mirrors so that they can highly efficient nano-focus X-rays [17].

The alignments of these focusing elements are carried out with two mounting stages for the sample and the focusing element, such as a mirror. In general, it is better that each stage has three dimensions of linear motion (x, y, z) and three directions of angular motion (θ_x, θ_y, θ_z) to allow a precise alignment for ideal focusing on a sample surface and to be compatible with any measurement methods. To scan over a wide area on a sample, one needs to prepare an appropriate stage with the precision control of the position and angle. Moreover, an X-ray having a wavelength on the order of 1 nm ($h\nu \sim 1$ keV), a so-called soft X-ray, requires vacuum conditions, and the stages must therefore be vacuum-compatible. Such a stage is typically quite expensive. The nano-focusing and soft X-ray spectroscopic mapping required for science and technology creates a strong demand for the design and development of a simple system that performs well at a reasonable cost.

In this technical note, we report our development of a simple scanning probe system for soft X-ray spectroscopy with a nano-focusing mirror [24] at a synchrotron radiation beamline. A set of two stages of a Wolter mirror and a sample requires only five degrees of freedom in total, three for the mirror and two for the sample. This simple configuration is made possible by two characteristics of the Wolter mirror. First, the Wolter mirror has a cylindrical shape so that it can focus the beam horizontally and vertically at the same time. It thus saves the number of stages compared to the case using the two plane-type mirrors (ex. KB mirrors) that focus the beam in the horizontal or vertical direction individually. Second, the focusing system with a Wolter mirror is rather error tolerant. In fact, the acceptable alignment error is hundreds to 1000 times larger than with the ellipsoidal mirror [20, 22, 23, 25], allowing easier alignment. With this setup, we achieved 800-nm focusing at $h\nu$ = 400 eV and successfully performed the chemical mapping of a mesh sample by taking signals of the X-ray absorption edges of Fe ($h\nu$ = 709.5 eV) and Al ($h\nu$ = 1560 eV). The present design and the actual system demonstrate that a nano-focusing unit with a mirror is no longer a luxury but can be reasonably installed on the beamline of synchrotron radiation or an X-ray free-electron laser.

II. INSTRUMENTS

A. Optical layout

The system was developed on the soft X-ray beamline, BL07LSU, at SPring-8 [4–6]. The light source of the beamline is a segmented cross undulator that is composed of four horizontal figure 8 undulators and four vertical figure 8 undulators. The beamline is equipped with an entrance-slitless variable-included-angle Monk-Gillieson mounting monochromator with a varied-line-spacing plane grating [4]. The optical layout is shown in Figure 1(a). The cylindrical mirror, M0, reflects the photon beam horizontally (x-direction) and focuses the beam vertically (z-direction) to the virtual focal point behind the grating. It is noted that the z-direction is the direction of energy dispersion and the exit slit, S2, is responsible for mechanically cutting the spectral beam, diffracted at the grating, for monochromatization. The bent cylindrical mirror, M1, reflects the beam horizontally (x-direction) and focuses it horizontally on the position of the exit slit (S2). To optimize the resolving power, the plane mirror, M2, varies with the grazing incident angle of the grating, Gr, in the angle range of 172°–178° through off-axis rotation. The soft X-ray beamline achieves high energy resolution ($E/\Delta E > 10000$) and high photon flux > 10^{12} photons s^{-1} (0.01% bandwidth)$^{-1}$ in the photon energy range $h\nu$ = 250–2000 eV with controllable and fast polarization switching [4–6].

An experimental station at the beamline is equipped with a set of post-focusing mirrors, a spherical or tangential mirror and a cylindrical or sagittal mirror [not shown in Figure 1(a)] [26]. The optical system was designed to generate a spot size of ~50 μm (x-direction) and < 10 μm (z-direction) at the sample position. Instead of using the current post-focusing mirror system at the beamline, we installed, as shown in Figure 1(a), a quadrant slit (4DS), S3, and a Wolter type-I mirror (Natsume Optical Corp.) at the station to produce a much smaller spot size. This Wolter mirror was developed for a soft X-ray ptychography system [24].

B. Measurement chamber

Figure 1(b) illustrates the measurement setup for a sample. A mirror stage generates motion along the longitudinal (y) axis and at angles along vertical and horizontal directions, θ_V and θ_H. It is noted that rotations of θ_V and θ_H can be regarded as the yawing angle and the pitching angle of a plane-type mirror, respectively [22]. The large error tolerance of the Wolter mirror allowed us to omit the x and z motional stages and instead tune the mirror x and z positions by externally moving the measurement chamber itself. The absence of the mirror x stage was compensated also by adjusting the M1 mirror, located upstream on the beamline [Figure 1(a)]. This is practically possible because the distance between the M1 mirror and the Wolter mirror is so long that an

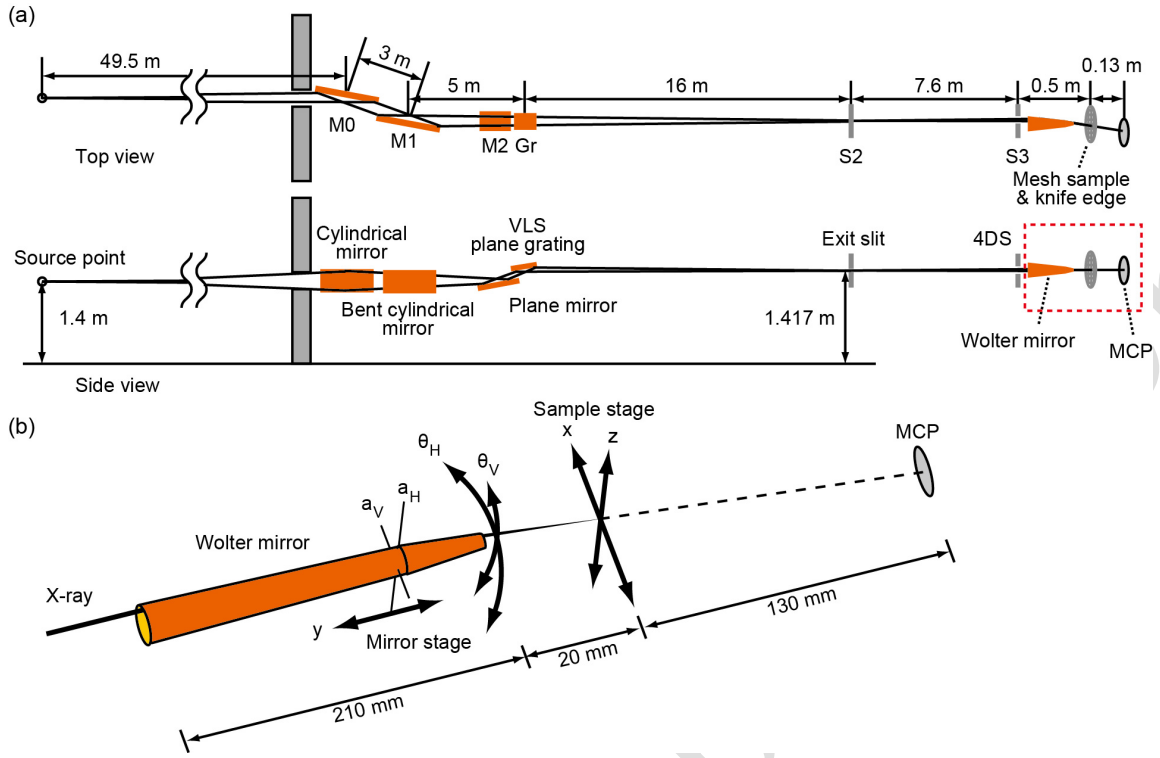

Figure 1: Optical layout of mirror focusing and sample scanning at SPring-8 BL07LSU. (a) Overall layout at the beamline comprising optical elements M0: cylindrical mirror, M1: bent cylindrical mirror, M2: plane mirror, Gr: plane grating with variable line spacing, S2: exit slit, and S3: a quadrant slit (4DS). A multi-channel plate (MCP) detector is placed downstream. (b) Layout of a mirror stage and sample stage. Directions of linear and angular motions are denoted x, y, z, θ_V, and θ_H. The rotation axes of θ_V and θ_H are denoted a_V and a_H.

angle change of the beam at the Wolter mirror essentially becomes lateral motion. A sample moves in the x and z directions, resulting in the mapping of a sample in the x–z space. As long as the angle of outgoing photons or electrons does not matter, rotational degrees of freedom can be abandoned. We also omitted the sample y motion by letting the mirror motions be solely responsible for tuning the focal position, which was made possible by the tolerance of the Wolter mirror. In total, only five degrees of freedom are needed in the present measurement system. The demagnification factor of the soft X-ray beam is approximately 115 ×, as determined by the ratio d_1/d_2, where d_1 is the distance between the exit slit and the boundary between ellipsoidal part and hyperboloidal part of the Wolter mirror, and d_2 is the distance between the boundary and sample. In the present system, the sample surface is set at 70 mm from the boundary, and the distance between the sample surface and the edge of the Wolter mirror is 20 mm, as shown in Figure 1(b). The space around the sample is large enough to add various experimental environments, such as cooling and heating environments. One can also conduct *operando* measurements with an applied current or electromagnetic field. In the experimental chamber, the photodetector of the multiple channel plate (MCP; F4655-14, Hamamatsu Photonics K. K.) is placed downstream to record beam profiles and make spectroscopy measurements. The MCP holder is painted with a fluorescent agent to make the optical alignment easier. Stage control and data acquisition for knife-edge scanning and two-dimensional (2D) mapping were performed with a homemade web-based application.

Figure 2 presents a collection of images of the experimental system at the end station. Figure 2(a) is a photograph of the vacuum chamber that connects to the beamline via a 4DS. The chamber is designed to be compact so that one can reduce the pumping time. During an experiment, the vacuum pressure is kept below 4×10^{-6} Pa with a turbo molecular pump. The chamber is mounted on a steel frame (colored red) that is filled with sand and protects against vibrations. Figure 2(b) is a photograph of the inside of the chamber. The Wolter mirror has a rotating body structure that is made of copper (Cu) and has an interior coated with gold (Au). The mirror is electrically isolated from the ground and attached to a cable that leads to an electrical feedthrough flange to connect with instruments outside the chamber. The top view of the system in Figure 2(c) shows the arrangement of the components in the chamber. All the parts are placed on an aluminum (Al) plate that is mounted on an ICF-356 flange. A part of the Wolter mirror is extended into the ICF-203 port of the vacuum chamber that is connected to the beamline side. Motions of the mirror stage and sample stage are controlled individually by an assembly of piezo stages, namely SLS-5252 (resolution of < 1 nm) and SR-5714C (resolution of < 1.5 μ°) manufactured by SmarAct GmbH for translational and rotational motions, respectively.

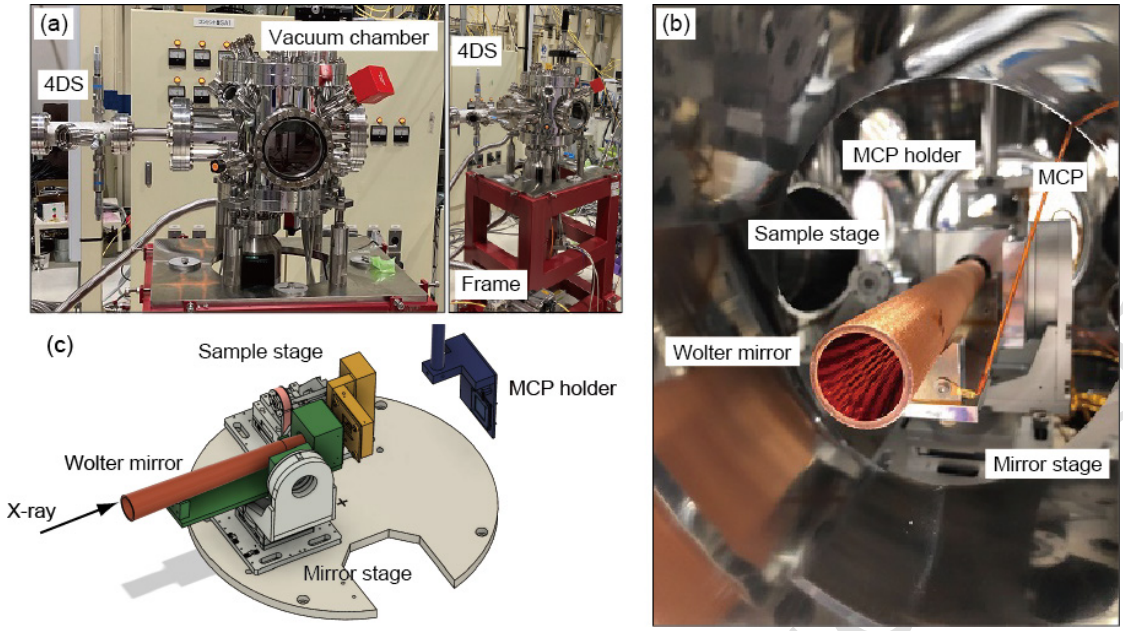

Figure 2: Experimental system. (a) Photograph of the vacuum chamber, mounted on a red frame, at the beamline. (b) Photograph of the inside of the chamber. (c) Three-dimensional CAD image of the setup in the chamber.

III. DEMONSTRATION

A. Spot profiling

The position of the measurement chamber and the rotational angle of M1 was tuned so that X-rays are reflected on the horizontal side of the Wolter mirror. The focal position was evaluated by the knife-edge scanning method using the Si knife-edge sample shown in Figure 3(a). The sample holder, made of Al, can move in the horizontal (x) and vertical (z) directions. While scanning the knife-edge sample, the appearance of the beam was monitored on the YAG:Ce scintillator mounted on the MCP holder to evaluate the deviation from the focal position. θ_H, θ_V, and y of the mirror were repeatedly tuned until the focal positions in the horizontal and vertical directions coincide at the sample position. The resulting focus size of the soft X-ray beam was evaluated by detecting the photon intensity at the MCP while scanning the knife-edge sample in the horizontal or vertical direction.

The focus size of the soft X-ray beam is evaluated by the knife-edge scanning method using the Si knife-edge sample shown in Figure 3(a). The sample holder, made of Al, can move in horizontal (x) and vertical (z) directions. Spot profiles are monitored by detecting the photon intensity at the MCP and by scanning the knife-edge sample in the horizontal or vertical direction. Figure 3(b, c) shows a set of intensity profiles, taken at hv = 400 eV and along the corresponding axis, x or z. The figure also presents differentiations of the curves. The line profiles indicate that the spot size of the soft X-ray beam is 2.7 μm along the x-axis and 0.8 μm along the z-axis, as evaluated by taking the full width at the half maximum of the differentiated peak.

B. Chemical mapping

2D mapping with the focused beam was demonstrated on a stainless steel (SUS) mesh (180 mesh, 140 μm/pitch) sample. Figure 4 shows images of the SUS mesh sample taken

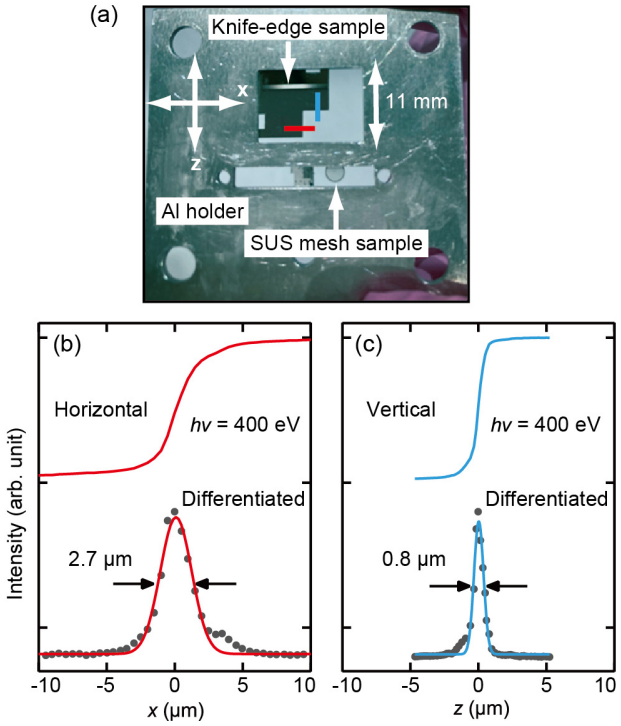

Figure 3: Knife-edge scans of the focused soft X-ray beam. (a) Photograph of an Al holder that mounts a knife-edge sample and a SUS mesh sample. (b, c) Line profiles and differentiation curves along horizontal (x) and vertical (z) directions.

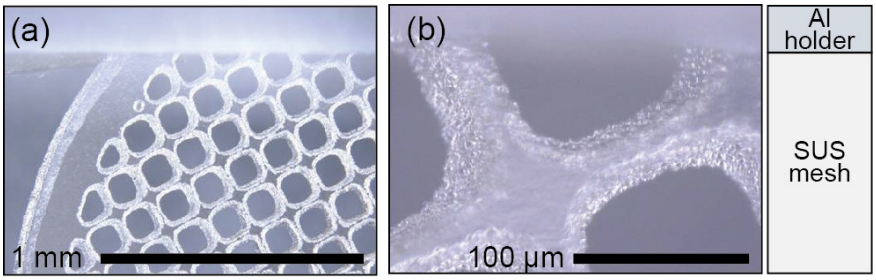

Figure 4: Al holder and SUS mesh sample. (a) Optical microscope image and (b) magnified image.

with an optical microscope. The SUS mesh is set on the Al holder shown in Figure 3(a). Photographs in Figure 4 cover the area of both the SUS mesh and Al holder. Figure 5(a–d) presents simultaneously recorded results of the total electron yield (TEY) and transmission for the same region of the sample in Figure 4(b). The spatial step size was 2 μm. The signal integration time per point was 1 s, and the total mapping time required to obtain the data in Figure 5(a) (101 × 121 pixels) was about 3.5 h.

The signals of the TEY were taken as the drain current of the sample whereas those of transmission were taken as the photon intensity at the MCP detector (Figures 1 and 2). As expected, the TEY and transmission maps appear inverted relative to one another because the photon beam is absorbed at the mesh grid (the TEY map) or transmits through the mesh holes (transmission map). Due to the short distance between the mirror and the sample, we observed that sample (mirror) drain current was contaminated by electrons photoemitted from the mirror (sample) surface. To overcome this difficulty, the Wolter mirror was electrically isolated from the ground to reduce the generation of photoelectrons by the charging effect at the mirror surface. Then, instead of using the mirror drain current to monitor the incident beam intensity (often referred to as I_0) for an absorption experiment, we monitored the drain current at a Au mesh placed upstream on the beamline. This procedure allowed the accurate evaluation of the sample drain current and incident-beam intensity for acquiring the TEY map. The results in Figure 5(a, b) were obtained for $h\nu$ = 709.5 eV, corresponding to the Fe L-shell absorption edge (the Fe L-edge). SUS contains Fe atoms, and the 2D map in Figure 5(a) thus shows a strong signal on the SUS mesh surface. This is further evidenced, as shown in Figure 5(e), by taking a line profile (Line 1) at the boundary between the SUS mesh and the Al holder.

The spectrum of the NEXAFS at the SUS mesh surface (Point 1) has clear peaks of the Fe L-edges. In contrast, this spectral feature is absent at the Al holder (Point 2). It is noted that the 2D intensity map in Figure 5(a) was taken at the Fe L-edge peak at $h\nu$ = 709.5 eV in the spectrum. The

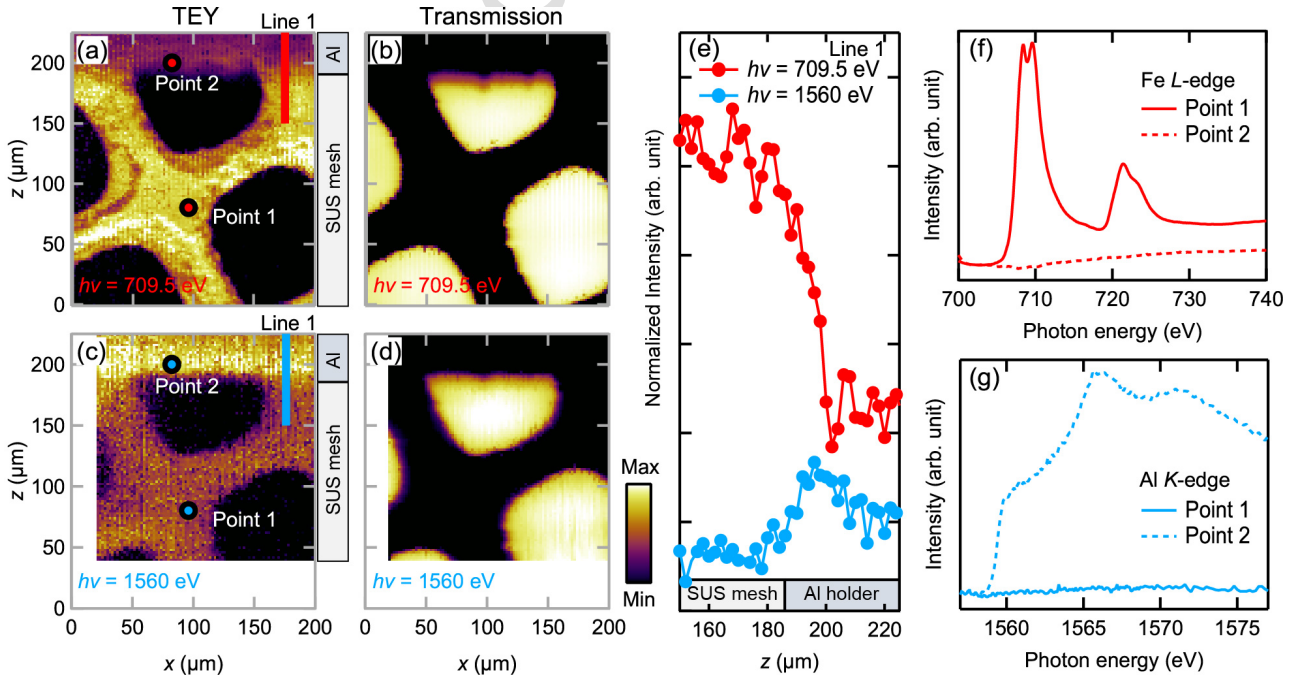

Figure 5: (a) 2D (x, z) TEY map and (b) 2D transmission map taken at $h\nu$ = 709.5 eV. (c) 2D TEY map and (d) 2D transmission map taken at $h\nu$ = 1560 eV. (e) One-dimensional line scans along Line 1 in (a, c). Arbitrary shifts have been given in the vertical direction for better visibility. (f) Fe L-edge NEXAFS spectra taken at Points 1 and 2. (g) Al K-edge NEXAFS spectra taken at Points 1 and 2.

NEXAFS signal depends on the element species and chemical state of the material, and the intensity distribution on the map thus includes such chemical information. In the case of the TEY map obtained for $h\nu$ = 1560 eV, the photon energy corresponds to a peak of the Al K-edge NEXAFS and the signal appears strong at the Al holder, as seen for the 2D map [Figure 5(c)], one-dimensional profile [Figure 5(e)], and point spectrum [Figure 5(g)].

The successful demonstration indicates that the present system of a nano-focusing mirror and 2D scanning stage is useful for characterizing a spatially non-uniform material or a microstructure with element and chemical information. The system can be combined with a robot unit for sample transfer and the mapping of a sample automatically or remotely. Moreover, the large space (20 mm) between the mirror and sample allows the installation of a sample environment for *operando* experiments [27], such as experiments involving gate voltages and current flow. The focusing mirror (the Wolter mirror) is made from Cu/Au, and the piezo stages are made from nonmagnetic components, and thus, it is possible to conduct mapping under a magnetic field (i.e., magnetic imaging). Using a polarization-controlled undulator [6, 27], the 2D chemical map becomes multidimensional, including the molecular orientation, orbital character, orbital magnetic moment, spin magnetic moment, and optical permittivity [6, 28–30]. The present design and the actual system are suited to experiments involving advanced soft X-ray spectroscopy [31, 32].

IV. CONCLUSION

We developed a compact, economic, and highly feasible system for X-ray spectroscopic mapping with a Wolter mirror. At the beamline, the mirror-sample unit requires only five degrees of freedom in an experiment, three for the mirror stage and two for the sample stage. We demonstrated 800-nm focusing of a soft X-ray beam and chemical mapping using the X-ray absorption edge of the elements on the SUS mesh sample. The present design and actual system are suited to experiments conducted with a nano-focused X-ray beam at beamlines of synchrotron radiation or an X-ray free-electron laser.

Acknowledgments

We thank Hisao Kiuchi, Koji, Horiba, Hiroto Motoyama, and Gota Yamaguchi for technical support and advice and Masaki Mizuguchi and Masaru Ikeda for preparing the sample. This work was supported by JST, CREST Grant No. JPMJCR21O4, Japan and by JSPS KAKENHI Grant Nos. 20H04451 and 21K20394, Japan. This work was carried out as joint research in the Synchrotron Radiation Research Organization and The Institute for Solid State Physics, The University of Tokyo (Proposal Nos. 2021A7402, 2021B7402, and 2022A7402). This work was also supported by "Nanotechnology Platform Japan" of the Ministry of Education, Culture, Sports, Science and Technology (MEXT). A part of this work was conducted at Takeda Clean Room/Ultrafine Lithography and Analysis Center of The University of Tokyo, supported by "Advanced Research Infrastructure for Materials and Nanotechnology in Japan (ARIM)", Grant Number JPMXP1222UT1008.

References

[1] J. Evans, *X-Ray Absorption Spectroscopy for the Chemical and Materials Sciences* (John Wiley & Sons, 2018).
[2] S. Hüfner, *Photoelectron Spectroscopy: Principles and Applications* (Springer Berlin, Heidelberg, 2003).
[3] J. Stöhr, *NEXAFS Spectroscopy* (Springer Berlin, Heidelberg, 1992).
[4] Y. Senba, S. Yamamoto, H. Ohashi, I. Matsuda, M. Fujisawa, A. Harasawa, T. Okuda, S. Takahashi, N. Nariyama, T. Matsushita, T. Ohata, Y. Furukawa, T. Tanaka, K. Takeshita, S. Goto, H. Kitamura, A. Kakizaki, and M. Oshima, Nucl. Instrum. Methods Phys. Res. A **649**, 58 (2011).
[5] S. Yamamoto, Y. Senba, T. Tanaka, H. Ohashi, T. Hirono, H. Kimura, M. Fujisawa, J. Miyawaki, A. Harasawa, T. Seike, S. Takahashi, N. Nariyama, T. Matsushita, M. Takeuchi, T. Ohata, Y. Furukawa, K. Takeshita, S. Goto, Y. Harada, S. Shin, H. Kitamura, A. Kakizaki, M. Oshima, and I. Matsuda, J. Synchrotron Radiat. **21**, 352 (2014).
[6] J. Miyawaki, S. Yamamoto, Y. Hirata, M. Horio, Y. Harada, and I. Matsuda, AAPPS Bull. **31**, 25 (2021).
[7] J. Avila and M. C. Asensio, Synchrotron Radiat. News **27** (2), 24 (2014).
[8] H. Iwasawa, P. Dudin, K. Inui, T. Masui, T. K. Kim, C. Cacho, and M. Hoesch, Phys. Rev. B **99**, 140510(R) (2019).
[9] C. Kastl, R. J. Koch, C. T. Chen, J. Eichhorn, S. Ulstrup, A. Bostwick, C. Jozwiak, T. R. Kuykendall, N. J. Borys, F. M. Toma, S. Aloni, A. Weber-Bargioni, E. Rotenberg, and A. M. Schwartzberg, ACS Nano **13**, 1284 (2019).
[10] K. Horiba, Y. Nakamura, N. Nagamura, S. Toyoda, H. Kumigashira, M. Oshima, K. Amemiya, Y. Senba, and H. Ohashi, Rev. Sci. Instrum. **82**, 113701 (2011).
[11] K. Yamauchi, M. Yabashi, H. Ohashi, T. Koyama, and T. Ishikawa, J. Synchrotron Radiat. **22**, 592 (2015).
[12] P. Dudin, P. Lacovig, C. Fava, E. Nicolini, A. Bianco, G. Cautero, and A. Barinov, J. Synchrotron Radiat. **17**, 445 (2010).
[13] U. Zastrau, C. Rödel, M. Nakatsutsumi, T. Feigl, K. Appel, B. Chen, T. Döppner, T. Fennel, T. Fiedler, L. B. Fletcher, E. Förster, E. Gamboa, D. O. Gericke, S. Göde, C. Grote-Fortmann, V. Hilbert, L. Kazak, T. Laarmann, H. J. Lee, P. Mabey, F. Martinez, K.-H. Meiwes-Broer, H. Pauer, M. Perske, A. Przystawik, S. Roling, S. Skruszewicz, M. Shihab, J. Tiggesbäumker, S. Toleikis, M. Wünsche, H. Zacharias, S. H. Glenzer, and G. Gregori, Rev. Sci. Instrum. **89**, 023703 (2018).
[14] R. J. Koch, C. Jozwiak, A. Bostwick, B. Stripe, M. Cordier, Z. Hussain, W. Yun, and E. Rotenberg, Synchrotron Radiat. News **31** (4), 50 (2018).
[15] S. Ulstrup, R. J. Koch, S. Singh, K. M. McCreary, B. T. Jonker, J. T. Robinson, C. Jozwiak, E. Rotenberg, A. Bostwick, J. Katoch, and J. A. Miwa, Sci. Adv. **6**, eaay6104 (2020).
[16] H. Motoyama, T. Sato, A. Iwasaki, Y. Takei, T. Kume, S. Egawa, K. Hiraguri, H. Hashizume, K. Yamanouchi, and H. Mimura, Rev. Sci. Instrum. **87**, 051803 (2016).
[17] H. Mimura, Y. Takei, T. Kume, Y. Takeo, H. Motoyama, S. Egawa, Y. Matsuzawa, G. Yamaguchi, Y. Senba, H. Kishimoto, and H. Ohashi, Rev. Sci. Instrum. **89**, 093104 (2018).
[18] H. Motoyama, S. Owada, G. Yamaguchi, T. Kume, S. Egawa, K. Tono, Y. Inubushi, T. Koyama, M. Yabashi, H. Ohashi, and H. Mimura, J. Synchrotron Radiat. **26**, 1406 (2019).

[19] G. Yamaguchi, H. Motoyama, S. Owada, Y. Kubota, S. Egawa, T. Kume, Y. Takeo, M. Yabashi, and H. Mimura, Rev. Sci. Instrum. **92**, 123106 (2021).
[20] S. Egawa, G. Yamaguchi, H. Motoyama, S. Owada, Y. Kubota, K. Tono, H. Ohashi, M. Yabashi, and H. Mimura, Proc. SPIE **11108**, 1110804 (2019).
[21] S. Egawa, S. Owada, H. Motoyama, G. Yamaguchi, Y. Matsuzawa, T. Kume, Y. Kubota, K. Tono, M. Yabashi, H. Ohashi, and H. Mimura, Opt. Express **27**, 33889 (2019).
[22] Y. Senba, H. Kishimoto, Y. Takeo, H. Yumoto, T. Koyama, H. Mimura, and H. Ohashi, J. Synchrotron Radiat. **27**, 1103 (2020).
[23] Y. Takeo, H. Motoyama, T. Shimamura, T. Kimura, T. Kume, Y. Matsuzawa, T. Saito, Y. Imamura, H. Miyashita, K. Hiraguri, H. Hashizume, Y. Senba, H. Kishimoto, H. Ohashi, and H. Mimura, Appl. Phys. Lett. **117**, 151104 (2020).
[24] T. Kimura, Y. Takeo, K. Sakurai, N. Furuya, S. Egawa, G. Yamaguchi, Y. Matsuzawa, T. Kume, H. Mimura, M. Shimura, H. Ohashi, I. Matsuda, and Y. Harada, Opt. Express **30**, 26220 (2022).
[25] Y. Takeo, H. Motoyama, T. Shimamura, T. Kimura, T. Kume, Y. Matsuzawa, T. Saito, Y. Imamura, H. Miyashita, K. Hiraguri, H. Hashizume, Y. Senba, H. Kishimoto, H. Ohashi, and H. Mimura, Proc. SPIE **11492**, 114920N (2020).
[26] M. Ogawa, S. Yamamoto, Y. Kousa, F. Nakamura, R. Yukawa, A. Fukushima, A. Harasawa, H. Kondoh, Y. Tanaka, A. Kakizaki, and I. Matsuda, Rev. Sci. Instrum. **83**, 023109 (2012).
[27] I. Matsuda, S. Yamamoto, J. Miyawaki, T. Abukawa, and T. Tanaka, e-J. Surf. Sci. Nanotechnol. **17**, 41 (2019).
[28] Y. Kudo, M. Horio, T. Sumi, T. Wada, Y. Hirata, T. Ohkochi, T. Kinoshita, and I. Matsuda, e-J. Surf. Sci. Nanotechnol. **20**, 124 (2022).
[29] Y. Kudo, Y. Hirata, M. Horio, M. Niibe, and I. Matsuda, Nucl. Instrum. Methods Phys. Res. A **1018**, 165804 (2021).
[30] Y. Kubota, Y. Hirata, J. Miyawaki, S. Yamamoto, H. Akai, R. Hobara, Sh. Yamamoto, K. Yamamoto, T. Someya, K. Takubo, Y. Yokoyama, M. Araki, M. Taguchi, Y. Harada, H. Wadati, M. Tsunoda, R. Kinjo, A. Kagamihata, T. Seike, M. Takeuchi, T. Tanaka, S. Shin, and I. Matsuda, Phys. Rev. B **96**, 214417 (2017).
[31] Y. Kubota, H. Motoyama, G. Yamaguchi, S. Egawa, Y. Takeo, M. Mizuguchi, H. Sharma, S. Owada, K. Tono, H. Mimura, I. Matsuda, and M. Yabashi, Appl. Phys. Lett. **117**, 042405 (2020).
[32] I. Matsuda and Y. Kubota, Chem. Lett. **50**, 1336 (2021).